Wave Motion 119 (2023) 103124

Contents lists available at ScienceDirect

Wave Motion

journal homepage: www.elsevier.com/locate/wamot

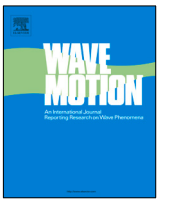

Transformation design of in-plane elastic cylindrical cloaks, concentrators and lenses

Michele Brun [a,*], Sébastien Guenneau [b]

[a] Dipartimento di Ingegneria Meccanica, Chimica e dei Materiali, Università di Cagliari, Cagliari I-09123, Italy
[b] UMI 2004 Abraham de Moivre-CNRS, Imperial College, London SW7 2AZ, UK

ARTICLE INFO

Article history:
Received 19 October 2021
Received in revised form 20 October 2022
Accepted 1 February 2023
Available online 21 February 2023

Keywords:
Cloaking
Anisotropic heterogeneous elastic media
Geometric transform
Numerical simulations

ABSTRACT

We analyse the elastic properties of a class of cylindrical cloaks deduced from linear geometric transforms $\mathbf{x} \rightarrow \mathbf{x}'$ in the framework of the Milton–Briane–Willis cloaking theory [New Journal of Physics 8, 248, 2006]. More precisely, we assume that the mapping between displacement fields $\mathbf{u}(\mathbf{x}) \rightarrow \mathbf{u}'(\mathbf{x}')$ is such that $\mathbf{u}'(\mathbf{x}') = \mathbf{A}^{-t}\mathbf{u}(\mathbf{x})$, where $\mathbf{A}$ is either the transformation gradient $F_{ij} = \partial x_i'/\partial x_j$ or the second order identity tensor $\mathbf{I}$. The nature of the cloaks under review can be three-fold: some of them are neutral for a source located a couple of wavelengths away; others lead to either a mirage effect or a field confinement when the source is located inside the concealment region or within their coated region (some act as elastic concentrators squeezing the wavelength of a pressure or shear polarized incident plane wave in their core); the last category of cloaks is classified as an elastic counterpart of electromagnetic perfect cylindrical lenses. The former two categories require either rank-4 elastic tensor and rank-2 density tensor and additional rank-3 and 2 positive definite tensors ($\mathbf{A} = \mathbf{F}$) or a rank-4 elasticity tensor and a scalar density ($\mathbf{A} = \mathbf{I}$) with spatially varying positive values. However, the latter example further requires that all rank-4, 3 and 2 tensors be negative definite ($\mathbf{A} = \mathbf{F}$) or that the elasticity tensor be negative definite (and non fully symmetric) as well as a negative scalar density ($\mathbf{A} = \mathbf{I}$). We provide some illustrative numerical examples with the Finite Element package Comsol Multiphysics when $\mathbf{A}$ is the identity.

1. Introduction

There has been a growing interest over the past years in the analysis of elastic waves in thin plates in the metamaterial community with the theoretical proposal [1,2], and its subsequent experimental validation [3,4] of a broadband cloak for flexural waves. Square [5] and diamond [6] cloaks are based on an improved transformed plate model, while form-invariance of the transformed equations in the framework of pre-stressed anisotropic plates is analized in [7–9].

There is currently a keen activity in transformation optics, whereby transformation based solutions to the Maxwell equations expressed in curvilinear coordinate systems travel along geodesics rather than in straight lines [10]. The fact that light follows shortest trajectories, the physical principle behind transformation optics, was formulated by de Fermat back in 1662. This minimization principle is applicable to ray optics, when the wavelength is much smaller than the size of the diffraction object. Leonhardt has shown in 2006 [11] that this allows for instance the design of invisibility cloaks using conformal mappings. Pendry, Schurig and Smith simultaneously reported that the same principle applies to

* Corresponding author.
E-mail address: mbrun@unica.it (M. Brun).

https://doi.org/10.1016/j.wavemoti.2023.103124

electromagnetic waves, i.e. when the wavelength is in resonance with the scattering object, by creating a hole in the curved space [12]. Interestingly, the mathematicians Greenleaf, Lassas and Uhlmann proposed an earlier route to invisibility using an inverse problem approach in 2003 [13], and together with Kurylev have been able since then to bridge the cloaking theory with Einstein theory of relativity, thereby suggesting possible avenues towards electromagnetic wormholes [14,15]. Leonhardt and Philbin have further proposed an optical fibre experiment [16] for an analogue of Hawking's famous event horizon in his theory of black holes [17]. It seems therefore fair to say that transformation optics offers a unique laboratory for thought experiments, leading to a plethora of electromagnetic paradigms. However, this would remain some academic curiosity without the practical side effect since the advent of so-called metamaterials, first introduced by Pendry in 1999 to obtain artificial magnetism in locally resonant periodic structures [18].

The first realization of an electromagnetic invisibility cloak [19] is a metamaterial consisting of concentric arrays of split-ring resonators. This structured material effectively maps a concealment region into a surrounding shell thanks to its strongly anisotropic effective permittivity and permeability which further fulfil some impedance matching with the surrounding vacuum. The cloak thus neither scatter waves nor induces a shadow in the transmitted field. Split ring resonators enable to meet among others the prerequisite artificial magnetism property, otherwise unobtainable with materials at hand [18]. This locally resonant micro-structured cloak was shown to conceal a copper cylinder around 8.5 GHz, as predicted by numerical simulations [19].

The effectiveness of the transformation based invisibility cloak was demonstrated theoretically by Leonhardt [11] solving the Helmholtz equation. Note that this equation is not only valid to compute ray trajectories (geodesics) in the geometrical optic limit, but also for matter waves in the quantum theory framework thanks to some mathematical correspondences between the Helmholtz and Schrödinger equations. Zhang et al. used this analogy to propose a quantum cloak based upon ultracold atoms within an optical lattice [20]. Greenleaf et al. subsequently discussed resonances (so-called trapped modes) occurring at a countable set of discrete frequencies inside the quantum cloak, using a spectral theory approach [21].

Using analogies between the Helmholtz and the Maxwell's equations, Cummer and Schurig demonstrated that pressure acoustic waves propagating in a fluid also undergo the same geometric transform in 2D [22]. Chen and Chan further extended this model to 3D acoustic cloaks [23], followed by an independent derivation of the acoustic cloak parameters in [24,25]. Such meta-fluids require an effective anisotropic mass density as in the model of Torrent and Sanchez-Dehesa [26]. However, an acoustic cloak for linear surface water waves studied experimentally and theoretically in [27], only involves an effective anisotropic shear viscosity.

Nevertheless, transformation based invisibility cloaks cannot be applied in general to elastodynamic waves in structural mechanics as there is a lack of one-to-one correspondence between the equations of elasticity and the Maxwell's equations [28]. Bigoni et al. actually studied such neutral inclusions in the elastostatic context using asymptotic and computational methods in the case of anti-plane shear and in-plane coupled pressure and shear polarizations [29], but when one moves to the area of elastodynamics, geometrical transforms become less tractable and neutrality breaks down: there are no conformal maps available in that case, and one has to solve inherently coupled tensor equations.

More precisely, Milton, Briane and Willis have actually shown that there is no symmetric rank-4 elasticity tensor describing the heterogeneous anisotropic medium required for an elastodynamic cloak in the context of Cauchy elasticity [28]. However, so-called Willis's equations, discovered by the British applied mathematician John Willis in the early 80's [30,31], offer a new paradigm for elastodynamic cloaking, as they allow for introduction of additional rank-3 and rank-2 tensors in the equations of motion that make cloaking possible.

Nevertheless, Brun, Guenneau and Movchan have shown [32] that it is possible to design an elastic cloak without invoking Willis's equations for in-plane coupled shear and pressure waves with a metamaterial described by a rank-4 elasticity tensor preserving the main symmetries, as well as a scalar density. Importantly, both elasticity tensor and density are inhomogeneous, and, at the inner boundary of the cloak, $C_{\theta\theta\theta\theta}$ is singular while density ρ' vanishes [32]. Some designs based on a homogenization approach for polar lattices has been proposed by Nassar, Chen and Huang [33] and Garau et al. [34]. Achaoui et al. have proposed an alternative design making use of elastic swiss-rolls [35]. Diatta and Guenneau [36] have shown that a spherical elastodynamic cloak can be designed using the same route as in [32], but the corresponding metamaterial design remains an open problem. There is an alternative, pre-stress, route to elastic cloaking proposed by Norris and Parnell that greatly relaxes constraints on material properties compared to the previous routes [37–39].

In the present article, we further investigate cylindrical cloaks for in-plane elastic waves using a radially symmetric linear geometric transform which depends upon a parameter. Depending upon the value of the parameter, the transform is applied to the design of neutral (invisibility) cloaks, elastic concentrators or cylindrical lenses. We discuss their underlying mechanism using a finite element approach which is adequate to solve the Navier equations in anisotropic heterogeneous media.

2. Governing equations and elastic properties of cloaks

2.1. The equations of motion

The propagation of in-plane elastic waves is governed by the Navier equations. Assuming time harmonic $\exp(-i\omega t)$ dependence, with ω as the wave frequency, allows us to work directly in the spectral domain. Such dependence is assumed

henceforth and suppressed, leading to

$$\nabla \cdot \mathbf{C} : \nabla \mathbf{u} + \rho\, \omega^2 \mathbf{u} + \mathbf{b} = \mathbf{0}\,, \tag{1}$$

where, considering cylindrical coordinates (r, θ), $\mathbf{u} = (u_r, u_\theta)$ is the in-plane displacement, ρ the density and C_{ijkl} $(i, j, k, l = r, \theta)$ the fourth-order elasticity tensor of the (possibly heterogeneous anisotropic) elastic medium. In Eq. (1) $\mathbf{b}$ is the body force.

2.2. The transformed equations of motion

Let us now consider the radial linear geometric transform $(r, \theta) \to (r', \theta')$, with $\theta' = \theta$, shown in Fig. 1

$$r' = \begin{cases} [(1+\alpha)r_1 - \alpha r_0]\frac{r}{r_0} & \text{for} \quad r' \le r'_0 \quad \text{(domain A)}, \\ (1+\alpha)r_1 - \alpha r & \text{for} \quad r'_0 \le r' \le r'_1 \quad \text{(domain B)}, \\ r & \text{for} \quad r' \ge r'_1 \quad \text{(domain C)}, \end{cases} \tag{2}$$

where $\alpha = -(r'_1 - r'_0)/(r_1 - r_0)$ is a real parameter and $r'_0 = (1+\alpha)r_1 - \alpha\, r_0$, $r'_1 = r_1$. The transformation gradient is $\mathbf{F} = (dr'/dr)\mathbf{I}_r + (r'/r)\mathbf{I}_\perp$ where $\mathbf{I}_r = \mathbf{e}_r \otimes \mathbf{e}_r$ is the second-order projection tensor along the radial direction identified by the unit vector $\mathbf{e}_r$, and $\mathbf{I}_\perp = \mathbf{I} - \mathbf{I}_r$, with $\mathbf{I}$ second-order identity tensor. Furthermore, $J = \det \mathbf{F}$ is the Jacobian of the transformation.

Design of in-plane transformation-based elastic cloaks was discussed in [32] when $\alpha = -1 + r'_0/r'_1$ ($r_0 = 0$): in that case, (2) simplifies into the geometric transform for an invisibility cloak $r' = r'_0 + \frac{r'_1 - r'_0}{r'_1} r$ in the domain (B) [12,13], where r'_0 and r'_1, respectively, denote the inner and outer radii of the circular cloak. However, other values of the parameter α lead to equally interesting cloaks, such as neutral concentrators, first studied in the context of electromagnetism [40], and we would like to discuss these in the sequel.

We now need to consider two cases for the transformed equations of motion.

2.2.1. Gauge transform $\mathbf{u}'(r', \theta') = \mathbf{u}(r, \theta)$

By application of transformation (2) with the Gauge $\mathbf{u}'(r', \theta') = \mathbf{u}(r, \theta)$ the Navier Eqs. (1) are mapped into the equations

$$\nabla' \cdot \mathbf{C}' : \nabla' \mathbf{u}' + \rho' \omega^2 \mathbf{u}' + \mathbf{b}' = \mathbf{0}\,, \tag{3}$$

where $\mathbf{u}'(r', \theta')$ and $\mathbf{b}'(r', \theta')$ are the transformed displacement and body force, respectively, and $\nabla' = \mathbf{F}^t \nabla$ the gradient operator in the transformed coordinates. In particular, we stress that we assume an identity gauge transformation [32,41], i.e. $\mathbf{u}'(r', \theta') = \mathbf{u}(r, \theta)$. The stretched density is the scalar field

$$\rho' = \begin{cases} \left[\dfrac{(1+\alpha)r'_1 - r'_0}{\alpha r'_0}\right]^2 \rho & \text{in A}, \\ \dfrac{r' - (1+\alpha)r'_1}{\alpha^2 r'}\rho & \text{in B}, \\ \rho & \text{in C}, \end{cases} \tag{4}$$

homogeneous in A and C. The transformed linear elasticity tensor has components

$$C'_{ijkl} = J^{-1} C_{mnop} F_{im} F_{ko} \delta_{jn} \delta_{lp}\,, \tag{5}$$

where $(i, j, k, l = r', \theta')$, $(m, n, o, p = r, \theta)$, δ_{jn} is the Kronecker delta and the usual summation convention over repeated indices is used. In particular, if before transformation the material is isotropic, i.e. $C_{ijkl} = \lambda \delta_{ij}\delta_{kl} + \mu(\delta_{ik}\delta_{jl} + \delta_{il}\delta_{jk})$ $(i, j, k, l = r, \theta)$, with λ and μ the Lamé moduli, the transformed elasticity tensor $\mathbf{C}'$ has non-zero cylindrical components

$$\begin{aligned} &C'_{r'r'r'r'} = \tfrac{r' - (1+\alpha)r_1}{r'}(\lambda + 2\mu), \quad && C'_{\theta'\theta'\theta'\theta'} = \tfrac{r'}{r' - (1+\alpha)r_1}(\lambda + 2\mu), \\ &C'_{r'r'\theta'\theta'} = C'_{\theta'\theta'r'r'} = \lambda, && C'_{r'\theta'\theta'r'} = C'_{\theta'r'r'\theta'} = \mu, \\ &C'_{r'\theta'r'\theta'} = \tfrac{r' - (1+\alpha)r_1}{r'}\mu, && C'_{\theta'r'\theta'r'} = \tfrac{r'}{r' - (1+\alpha)r_1}\mu\,, \end{aligned} \tag{6}$$

in B and $\mathbf{C}' = \mathbf{C}$ in A and C.

The transformation and the corresponding transformed density ρ' and elasticity tensor $\mathbf{C}'$ are broadband, they do not depend on the applied frequency ω.

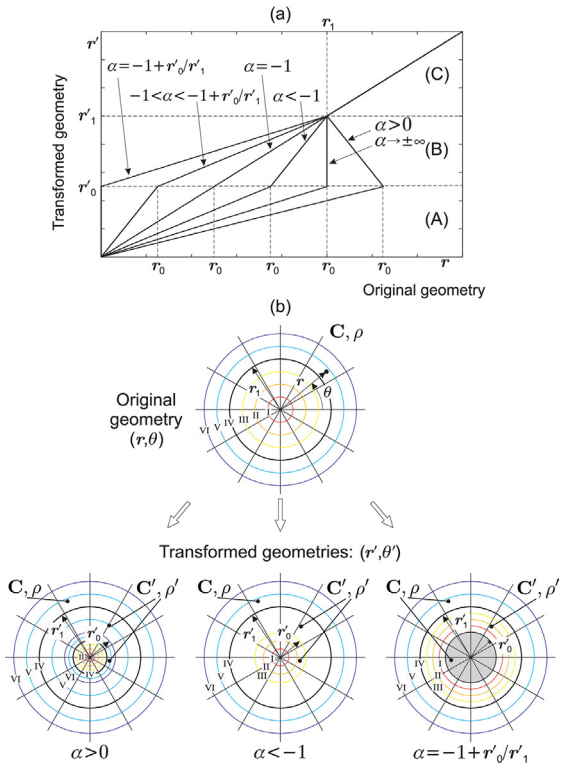

Fig. 1. Geometric transform of Eq. (2). (a) Representation of the transform $r \to r'$ for different values of the parameter α. The domains A ($r' \le r'_0$), B ($r'_0 \le r' \le r'_1$) and C ($r' \ge r'_1$) are indicated. (b) Transformation of the geometry for $\alpha > 0$, $\alpha < -1$ and $\alpha = -1 + r'_0/r'_1$ (perfect cloak).

2.2.2. Gauge transform $\mathbf{u}'(r', \theta') = \mathbf{F}^{-t}\mathbf{u}(r, \theta)$

As noted in [28], by application of transformation (2) with the Gauge $\mathbf{u}'(r', \theta') = \mathbf{F}^{-t}\mathbf{u}(r, \theta)$, where $\mathbf{F}$ is the transformation gradient, the Navier Eqs. (1) are mapped into the equations

$$\nabla' \cdot \left(\mathbf{C}'' : \nabla' \mathbf{u}' + \mathbf{D}' \cdot \mathbf{u}' \right) + \mathbf{S}' : \nabla' \mathbf{u}' + \omega^2 \rho' \mathbf{u}' + \mathbf{b}' = \mathbf{0}. \tag{7}$$

The transformed rank-4 elasticity tensor $\mathbf{C}''$ has components

$$C''_{ijkl} = J^{-1} F_{im} F_{jn} C_{mnop} F_{ko} F_{lp} \ , \tag{8}$$

where $(i, j, k, l = r', \theta')$, $(m, n, o, p = r, \theta)$.

We note that $\mathbf{C}''$ in (8) has all the symmetries, unlike $\mathbf{C}'$ in (6), which has the major but not the minor symmetries.

The rank-3 tensors $\mathbf{D}'$ and $\mathbf{S}'$ in (8) have elements

$$D'_{ijk} = J^{-1} F_{im} F_{jn} C_{mnop} \frac{\partial^2 x'_k}{\partial x_o \partial x_p} = D'_{jik} \ , \tag{9}$$

and

$$S'_{ijk} = J^{-1} \frac{\partial^2 x'_i}{\partial x_m \partial x_n} C_{mnop} F_{jo} F_{kp} = S'_{jik}. \tag{10}$$

Finally, the transformed density ρ' in (8) is matrix valued

$$\rho'_{ij} = J^{-1} \rho F_{im} F_{jm} + J^{-1} \frac{\partial^2 x'_i}{\partial x_m \partial x_n} C_{mnop} \frac{\partial^2 x'_j}{\partial x_o \partial x_p} = \rho'_{ji}. \tag{11}$$

These expressions were first derived in [28].

Now, if before transformation the material is isotropic, then the transformed elasticity tensor $\mathbf{C}''$ has non-zero cylindrical components

$$\begin{aligned}
&C''_{r'r'r'r'}=\tfrac{r'-(1+\alpha)r_1}{r'(r_1-r_0)^2}(\lambda+2\mu),\\
&C''_{\theta'\theta'\theta'\theta'}=\tfrac{r'^3}{(r_1-r_0)^2(r'-(1+\alpha)r_1)^3}(\lambda+2\mu),\\
&C''_{r'r'\theta'\theta'}=C''_{\theta'\theta'r'r'}=\tfrac{r'}{(r_1-r_0)^2(r'-(1+\alpha)r_1)}\lambda,\\
&C''_{r'\theta'\theta'r'}=C'_{\theta'r'r'\theta'}=C''_{r'\theta'r'\theta'}=C''_{\theta'r'\theta'r'}=\tfrac{r'}{(r_1-r_0)^2(r'-(1+\alpha)r_1)}\mu\ ,
\end{aligned} \tag{12}$$

in B and $\mathbf{C}''=\mathbf{C}$ in A and C.

On the other hand, the rank-3 tensors $\mathbf{D}'$ and $\mathbf{S}'$ have non-zero cylindrical components

$$\begin{aligned}
&D'_{r'r'r'}=\tfrac{1}{(r_1-r_0)^2(r'-(1+\alpha)r_1)(r'+r_1r_0/(r_1-r_0))}\lambda=-S'_{r'r'r'}\\
&D'_{r'\theta'\theta'}=D'_{\theta'r'\theta'}=2\tfrac{1}{(r_1-r_0)^2(r'-(1+\alpha)r_1)^2}\mu=-S'_{\theta'\theta'r'}=-S'_{\theta'r'\theta'}\\
&D'_{\theta'\theta'r'}=\tfrac{r'+r_1r_0/(r_1-r_0)}{(r_1-r_0)^2(r'-(1+\alpha)r_1)^3}(2\mu+\lambda)=-S'_{r'\theta'\theta'}.
\end{aligned} \tag{13}$$

Similar expressions can be derived for the transformed density. Expressions in (12) and (13) are more intricate than those in (6); thus, in the sequel, we focus on the transformed equations of motion (3).

2.3. Interface conditions for gauge $\mathbf{u}'(r',\theta')=\mathbf{u}(r,\theta)$

Perfect cloaking and perfect concentrator require additional conditions on displacements and tractions at the interfaces between the domains with different material properties introduced by the transformation (2). In the transformed problem (3) there are two interfaces, between domains A and B, at $r'=r'_0$ and $r=r_0$, and at the cloak's outer boundary, between domains B and C, at $r'=r=r_1$. Transformed equations (3) together with the assumption $\mathbf{u}'(r',\theta')=\mathbf{u}(r,\theta)$ assure that displacements and tractions in the inhomogeneous transformed domain at a point (r',θ') coincide with displacements and tractions at the corresponding point (r,θ) in the original homogeneous problem (1) where no interfaces between different materials are present. In particular, if we introduce the Cauchy stress tensors $\boldsymbol{\sigma}'=\mathbf{C}':\nabla'\mathbf{u}'$ and $\boldsymbol{\sigma}=\mathbf{C}:\nabla\mathbf{u}$ for the transformed and original problem, respectively, it is verified the following equality between tractions

$$\boldsymbol{\sigma}'\cdot\mathbf{e}'_r=\boldsymbol{\sigma}\cdot\mathbf{e}_r, \tag{14}$$

at $r'=r'_0$, $r=r_0$ and at $r'=r=r_1$. Equality (14) can be easily demonstrated by using Nanson's formula [42] $\mathbf{e}'_r=J\mathbf{F}^{-t}\mathbf{e}_r$ for the radial unit vectors.

Note that the matching is independent on the particular value assumed by α.

2.4. Perfect cloak. Singularity at the inner interface

We note that for the perfect cloak [32], i.e. $r_0=0$ and $\alpha=-1+r'_0/r'_1$, a point at $r=0$ is mapped into a disc of radius r'_0. This is a singular transformation and, at the cloak inner boundary, $r'-(1+\alpha)r_1\to 0$. Therefore, at $r'=r'_0$, from (4) and (6) one can see that $\rho'\to 0$, $C'_{r'r'r'r'}$, $C'_{r'\theta'r'\theta'}\to 0$, while $C'_{\theta'\theta'\theta'\theta'}$, $C'_{\theta'r'\theta'r'}\to\infty$.

Similarly, at $r'=r'_0$, from (12) and (13) one can see that $C''_{r'r'r'r'}\to 0$, while $C''_{\theta'\theta'\theta'\theta'}$, $C''_{r'r'\theta'\theta'}=C''_{\theta'\theta'r'r'}$, $C''_{r'\theta'\theta'r'}=C'_{\theta'r'r'\theta'}=C''_{r'\theta'r'\theta'}=C''_{\theta'r'\theta'r'}\to\infty$. Moreover, one notes that the rate of divergence is faster for $\mathbf{C}''$ than $\mathbf{C}'$, and thus anisotropy is even more extreme in the neighbourhood of the inner boundary for $\mathbf{C}''$. All expressions in (13) diverge when $r'-(1+\alpha)r_1\to 0$.

The required extreme anisotropy physically means that pressure and shear waves propagate with an infinite velocity in the azimuthal θ'-direction and zero velocity in the radial r'-direction along the inner boundary, which results in a vanishing phase shift between a wave propagating in a homogeneous elastic space and another one propagating around the coated region.

Clearly the presence of unbounded physical properties poses limitations on possible realizations and numerical implementation of the model; regularization techniques have been proposed introducing the concept of *near cloak* [43–45], but the realization of such elastodynamic cloaks remains a challenge.

2.5. General transformation

We now wish to extend first the proposal of Rahm et al. [40] of an omni-directional electromagnetic concentrator to the elastic setting and second to consider a more general transformation including folded transformed geometries, as proposed for quasi-static equations of electromagnetism by Milton et al. [46]. We recall that the transformation (2) compresses/expands a disc with radius r_0 at the expense of an expansion/compression of the annulus between r_0 and r_1. The inner disc is expanded for $-1<\alpha<-1+r'_0/r'_1$ with the limiting cases $\alpha=-1$ corresponding to an identity ($r'_0=r_0$) and $\alpha=-1+r'_0/r'_1$ to perfect cloaking. On the contrary the disc is compressed, namely $r'_0>r_0$, for $\alpha<-1$ and $\alpha>0$. Additionally, when $\alpha>0$, $r_0>r_1$ and a folding of the original geometry is obtained.

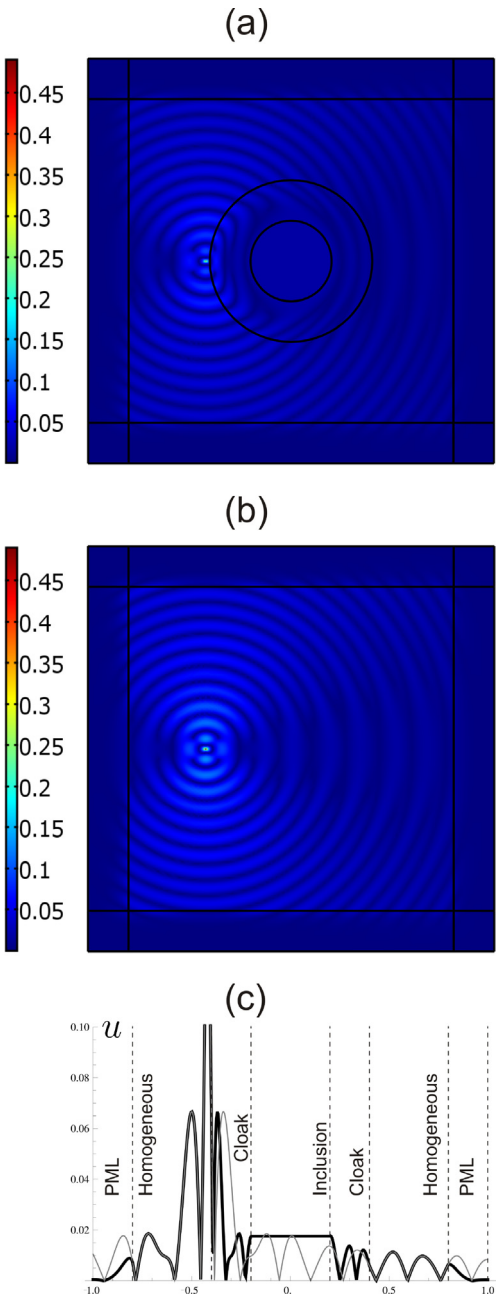

Fig. 2. Elastic field generated by an horizontal unit force applied in the external homogeneous region; $\alpha = -1 + r_0'/r_1' = -0.5$, $\omega d/c_s = 40$, source position $\mathbf{x}_0 = (-0.42, 0)d$. Magnitude $u = \sqrt{u_1^2 + u_2^2}$ of the displacement field in the system with (a) inclusion and cloaking and (b) in a homogeneous system. (c) Comparison between the displacement magnitude u computed in Comsol for a cloaked inclusion (black line) and the analytical Green's function in an infinite homogeneous linear elastic and isotropic material (grey line), see Eq. (17).

The material remains homogeneous and isotropic in the inner disc A where only the density is changed. In the annulus region B the material is heterogeneous and elastically anisotropic. Consistently with Brun et al. [32] and differently from Milton et al. [28] the density remains a scalar field (see also [41]). We stress that the heterogeneity is smoothly distributed and the material is functionally graded with the absence of any jump in the material properties leading to possible scattering effects. As detailed above, the interface conditions are automatically satisfied and do not introduce any scattering.

It is important to note that, excluding the perfect cloaking case, for bounded values of α all the elastic rigidities and the density are bounded leading to possible physical and numerical implementation of the metamaterial structure.

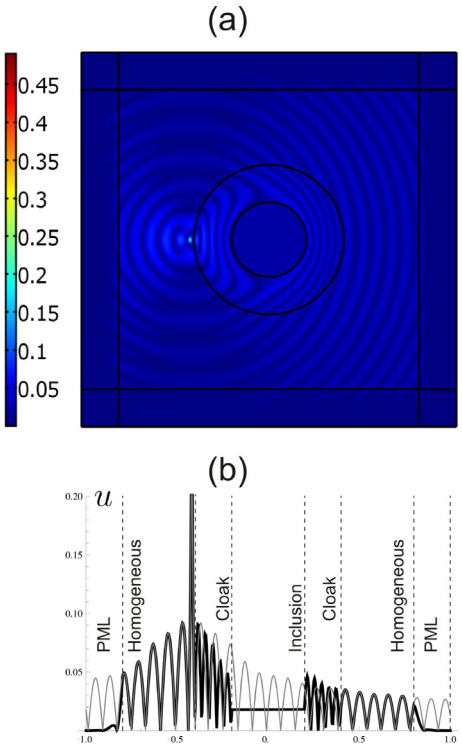

Fig. 3. Elastic field generated by a vertical unit force applied in the external homogeneous region. $\alpha = -1 + r_0'/r_1' = -0.5$, $\omega d/c_s = 40$, source $\mathbf{x}_0 = (-0.42d, 0)$. (a) Magnitude u of the displacement field; (b) Comparison between the displacement magnitude u computed in Comsol for a cloaked inclusion (black line) and the analytical Green's function in an infinite homogeneous linear elastic and isotropic material (grey line).

2.6. The radial field concentrator. Unbounded α

The limiting cases $\alpha \to \pm\infty$, where $r_0 = r_1$, correspond asymptotically to the radial transformation

$$r' = \begin{cases} \frac{r}{r_1} & \text{in A,} \\ r_1 & \text{in B,} \\ r & \text{in C.} \end{cases} \tag{15}$$

In such a case in the annulus region B $C'_{\theta'\theta'\theta'\theta'}$, $C'_{\theta'r'\theta'r'} \to \infty$, $\rho' \to \infty$ and all the other elastic rigidities components are unchanged. In such material, independently on the external field impinging the metamaterial region $r' \leq r_1'$, the elastic fields in B are radially independent and depend only on the azimuthal coordinate θ'. However, the harmonic behaviour cannot be reached in a finite time after the transient regime since the density ρ' is unbounded.

3. Numerical results and discussion

In this section, we report the finite element computations performed in the COMSOL multiphysics package. Normalized material parameters are used. A cloak of density ρ' (Eq. (4)) and elasticity tensor $\mathbf{C}'$ (Eqs. (5) and (6)) is embedded in an infinite isotropic elastic material with normalized Lamé moduli $\lambda = 2.3$ (GPa) and $\mu = 1$ (GPa), that corresponds to a Poisson ratio $\nu = 0.3485$ and a Young's to shear modulus ratio $E/\mu = 2.6966$, and mass density $\rho = 1$ kg/m^3. The cloak has inner and outer radii $r_0' = 0.2$ (m) and $r_1' = 0.4$ (m), respectively. The disc inside the cloak consists of the same elastic material as the outer medium but different density. We further consider a harmonic unit concentrated force applied either in the direction x_1 or x_2 which vibrates with a normalized angular wave frequency $\omega d/c_s = 40$, where c_s is the shear wavespeed (m/s) and d is a unit length (m). This force is sometimes located outside the cloak (cf. Figs. 2–4), sometimes inside the coating (cf. Fig. 5) or within the central disc (cf. Fig. 6), depending upon whether we are looking for some neutrality feature, lensing/mirage effect or some localization.

Before we start looking at the cloak's features depending upon the ranges of values of the parameter α, we briefly discuss the implementation of elastic perfectly matched layers (PMLs), in the framework of transformation elasticity.

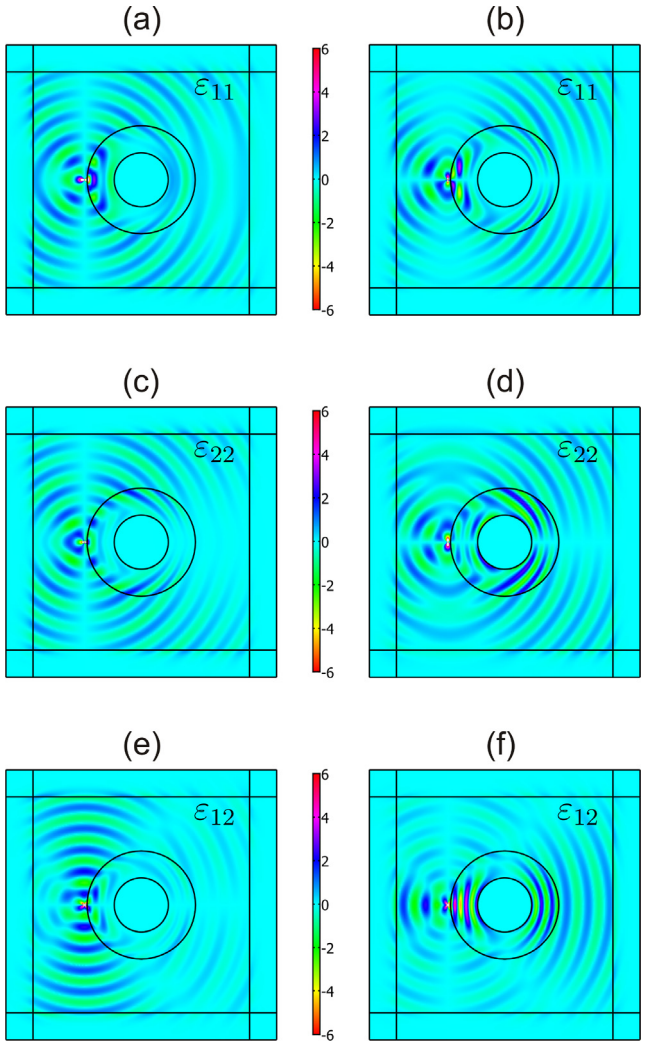

Fig. 4. Elastic deformation fields generated by a unit force applied in the external homogeneous region. $\alpha = -1 + r_0'/r_1' = -0.5$, $\omega d/c_s = 40$, source $\mathbf{x}_0 = (-0.42, 0)d$. (a), (c), (e) Force applied in the horizontal direction x_1. (b), (d), (f) Force applied in the vertical direction x_2. (a), (b) Component $\varepsilon_{11} = \frac{\partial u_1}{\partial x_1}$; (c), (d) Component $\varepsilon_{22} = \frac{\partial u_2}{\partial x_2}$; (e), (f) Component $\varepsilon_{12} = \varepsilon_{21} = \frac{1}{2}(\frac{\partial u_1}{\partial x_2} + \frac{\partial u_2}{\partial x_1})$.

3.1. Implementation of elastic cylindrical PMLs

A perfectly matched layer has been implemented in order to model the infinite elastic medium surrounding the cloak (cf. outer ring in Figs. 2–6); this has been obtained by application of the geometric transform [47],

$$x_i'' = (1 + a)\hat{x}_i - a x_i, \qquad i = 1, 2, \tag{16}$$

for $|x_i| > |\hat{x}_i|$, where a is now a complex number whose imaginary part accounts for the decay of the elastic waves and $\hat{x}_i = \pm 1$ in Figs. 2–6. The corresponding (complex) density ρ''' and elasticity tensor $\mathbf{C}'''$ are still given by (4) and (6). The accuracy of the PMLs has been numerically validated when $a = i - 1$, by comparison with the Green's function in homogeneous elastic space (cf. Eq. (17) and Fig. 2b, c).

We can therefore confidently carry out computations with these PMLs. We start by the study of an invisibility cloak for in-plane elastic waves, whereby the point source considered in [32] now lies in the close vicinity of the cloak (intense near field limit when the acoustic ray picture breaks down).

3.2. Neutrality for a point source outside the cloak

We report in Figs. 2 and 3 the computations for a point force applied at a distance $r = 0.42d$ away from the centre of the cloak and close to the cloak itself of outer radius $r_1' = 0.4d$. The force is applied in the horizontal direction in Fig. 2 and

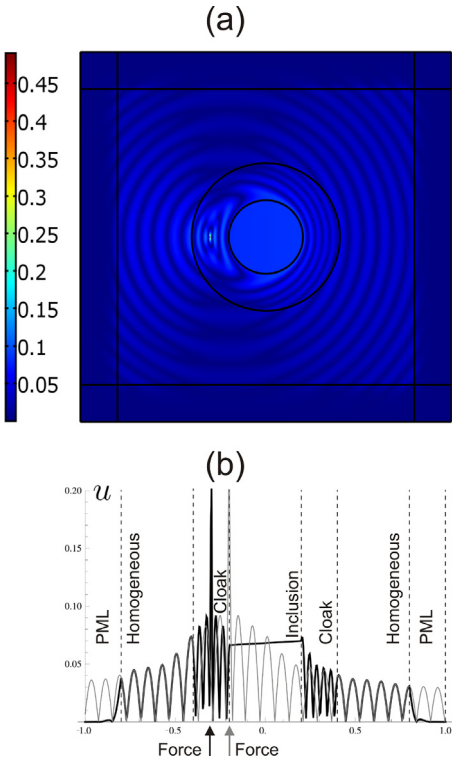

Fig. 5. Elastic field generated by a vertical unit force applied in the cloaking region. $\alpha = -1 + r_0'/r_1' = -0.5$, $\omega d/c_s = 40$, source $\mathbf{x}_0 = (-0.3, 0)d$. (a) Magnitude u of the displacement field; (b) Comparison between the displacement magnitude u computed in Comsol for a cloaked inclusion (black line) and the analytical Green's function in an infinite homogeneous linear elastic and isotropic material (grey line), corresponding to a force applied to a shifted source point $\mathbf{x}_0 = (-0.2, 0)d$.

in the vertical direction in Fig. 3. In both upper panels (a), we clearly see that both the wave patterns of the magnitude of the displacement field are smoothly bent around the central region within the cloak (where the magnitude is uniform).

The comparative analyses between panels (a) and (b) of Fig. 2 shows that the wave patterns in the external homogeneous domain are not perturbed by the presence of the inclusion and cloaking interface. This is verified quantitatively in Fig. 2 panel (c) and in Fig. 3 panel (b) where the numerically computed wave pattern is compared with the Green's function in the homogeneous elastic space

$$\mathbf{G}(\mathbf{x}) = \frac{i}{4\mu}\left\{H_0^{(1)}(k_s r)\mathbf{I} - \frac{Q}{\omega^2}\nabla\nabla\left[H_0^{(1)}(k_s r) - H_0^{(1)}(k_p r)\right]\right\}, \tag{17}$$

with $H_0^{(1)}$ the Hankel function, $\mathbf{I}$ the second order identity tensor, ∇ the gradient operator, $k_p = \omega/c_p$, $k_s = \omega/c_s$, $Q = (1/c_p^2 + 1/c_s^2)^{-1}(\lambda + \mu)/(\lambda + 2\mu)$, $c_p = \sqrt{(\lambda + 2\mu)/\rho}$, $c_s = \sqrt{\mu/\rho}$. The plots are reported along the horizontal line $x_2 = 0$ passing from the point of application of the force. The absence of forward or backward scattering is demonstrated by the excellent agreement between the two fields in the external homogeneous domain $r > 0.4$. Clearly, the profile is much different when the coating is removed and the inner disc is clamped or freely vibrating. We also see that the field in the cloaking region has the same amplitude as the one in homogeneous case, but shifted following the transformation $r'(r)$; in the inner disc the field is homogeneous. Finally the effectiveness of the PML domains can also be appreciated.

In Fig. 4 the deformation fields are also reported for both cases, where the force is applied in horizontal (first column) and vertical (second column) direction. In the upper (a, b) and central (c, d) panels the skew-symmetric nature of the components ε_{11} and ε_{22} of the deformation tensor reveals the tensor nature of the problem. The component ε_{12} leads to a non-intuitive pattern whereby fully-coupled shear and pressure components create the optical illusion of interferences. Again, the effect of the cloaking is shown and also for deformation fields waves are bent around the cloaking region without backward and forward scattering.

3.3. Mirage effect for a point source in the coating

In this section, we look at the case of a point force located inside the coating. In a way similar to what was observed for an electromagnetic circular cylindrical cloak [48], we observe in Fig. 5 a mirage effect: the point force seems to radiate

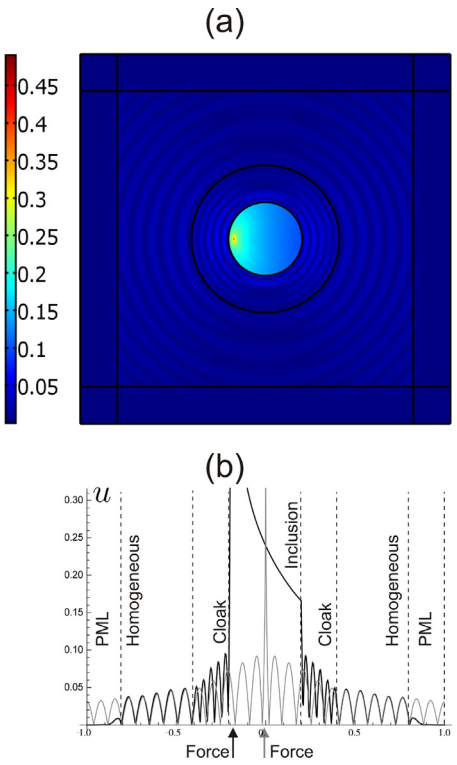

Fig. 6. Elastic field generated by a vertical unit force applied in the internal inclusion. $\alpha = -1 + r_0'/r_1' = -0.5$, $\omega d/c_s = 40$, $\mathbf{x}_0 = (-0.17, 0)d$. (a) Magnitude u of the displacement field; (b) Comparison between the displacement magnitude u computed in Comsol for a cloaked inclusion (black line) and the analytical Green's function in an infinite homogeneous linear elastic and isotropic material (grey line). The sources are located at $\mathbf{x}_0 = (-0.17, 0)d$ for the cloaked inclusion and at $\mathbf{x}_0 = (0, 0)d$ for the homogeneous system.

from a location shifted towards the inner boundary (further away from an observer) as given by

$$r = \frac{(1+\alpha)r_1 - r'}{\alpha}\ ,\ \theta = \theta'\ , \tag{18}$$

as also shown in panel (b).

Importantly, the profile of the shifted point source in homogeneous elastic space is superimposed with that of the point source located inside the coating, but only outside the cloak. In the invisibility region i.e. the disc at the centre of the cloak, the field is constant and this suggests that the central region behaves as a cavity. We study this cavity phenomenon in the next section.

The example in Fig. 5 reveals that any object located inside the coating would appear as a different elastic material with a different shape to an observer.

3.4. Confinement for a point source in the central region

We now consider a point force inside the invisibility region. Interestingly, a point source located in the invisibility zone always radiates outside the cloak as if it was located at the origin and this is quite natural as the central disc is simply the image of the origin via the geometric transform (18), as shown in Fig. 6. The fact that the central disc behaves as a closed cavity is also intuitive, as the elasticity tensor $\mathbf{C}'$ is singular on the boundary of the disc. We refer the reader to [21] for a discussion of almost-trapped eigenstates in a similar configuration for matter waves.

3.5. Squeezing the wavelength with an elastic concentrator

We report the effects associated to an increase in the magnitude of the parameter α describing the linear transformation (2). In Fig. 7 the effect of the cylindrical coating on the inclusion is given for a pressure plane wave $\mathbf{u} = (A\exp(ik_p t), 0)$ propagating in the horizontal direction x_1. A decrease of α from $\alpha = -1 + r_0'/r_1' = -0.5$ introduces wave propagation within the inclusion with progressive shorter wavelengths while the amplitude of the wave remains unchanged. From Fig. 7 panel (d) it is evident that, when $\alpha < -1$, the interface acts as an energy concentrator within the inclusion increasing

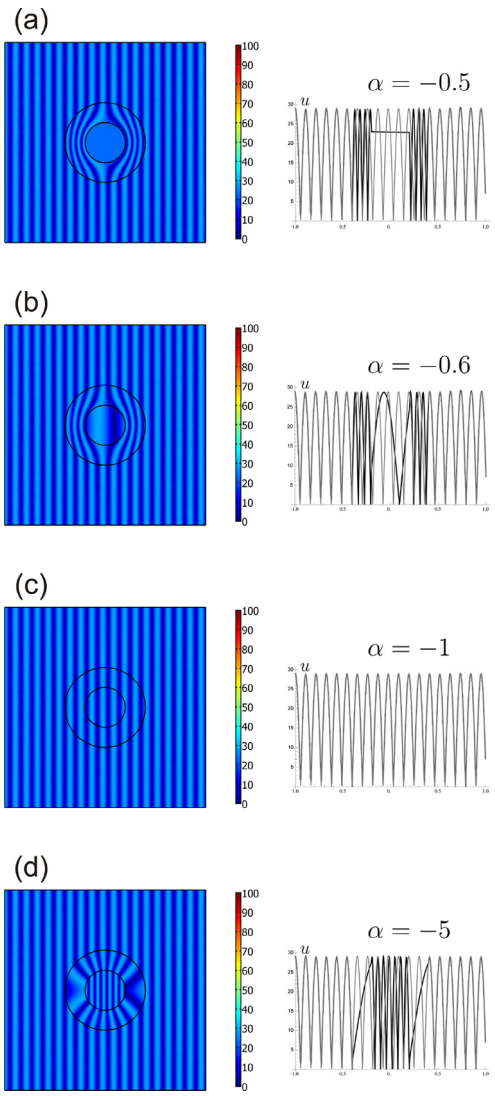

Fig. 7. Elastic field generated by a pressure plane wave $\mathbf{u} = (A\exp(ik_p t), 0)$ with $\omega d/c_s = 60$. Left column: magnitude u of the displacement field. Right column: comparison between the displacement magnitude u computed in Comsol for a cloaked inclusion (black line) and the pressure plane wave in an infinite homogeneous linear elastic and isotropic material (grey line), results are plotted along an horizontal line passing from the centre of the inclusion. (a) $\alpha = -0.5$, (b) $\alpha = -0.6$, (c) $\alpha = -1$, (d) $\alpha = -5$.

the energy flux. The energy crossing the inclusion region $r \leq r_0' = 0.2$d equals the energy crossing the larger region $r \leq r_0$, in a homogeneous material. In the interval $-1 > \alpha > -\infty$, $r_0' < r_0 < r_1'$.

We also note that, when $\alpha \neq -0.5$ the transformation is regular and material parameters remain bounded indicating additional advantages in technological and numerical implementations of the model. Last but not least, the field in the external domain remains unchanged.

3.6. Folding transformation. Superconcentration of an elastic wave with a cylindrical lens

We finally report in Fig. 8 an enhanced energy concentration effect obtained from a folding transformation ($\alpha > 0$). In such a case all the energy crossing a circular region larger than the region delimited by the cloaking interface is concentrated into the core. In Fig. 8, $\alpha = 0.94$ and the radius of the circular region in the homogeneous space is 3.06 times the radius of the inner inclusion. Again, such an effect is obtained by an increase in the energy flux, due to the shrinking of the wavelength, leaving unperturbed both the wave amplitude and the fields in the external region. At the interfaces between the core and the shell and between the shell and the matrix, we also note perturbations of the displacement field, associated to the anomalous resonance induced by the negative definite constitutive tensor $\mathbf{C}'$ in the shell [46,49,50].

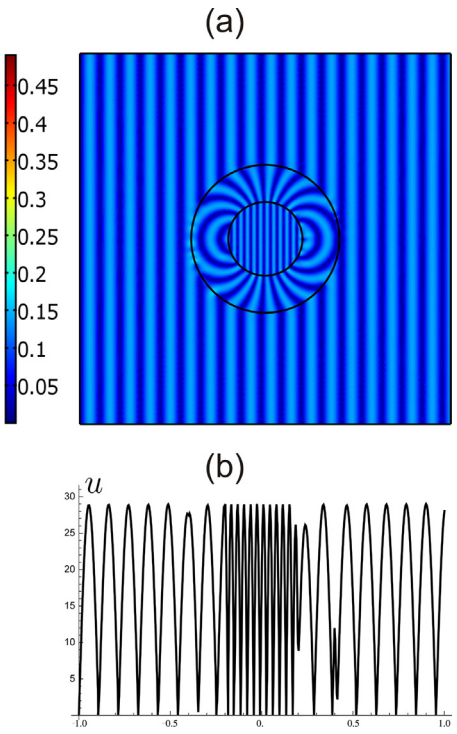

Fig. 8. Elastic field generated by a pressure plane wave $\mathbf{u} = (A\exp(ik_p t), 0)$ with $\omega d/c_s = 60$ and $\alpha = 0.94$. (a) Magnitude u of the displacement field. (b) Displacement magnitude u computed in Comsol for a cloaked inclusion plotted along an horizontal line passing from the centre of the inclusion.

Interestingly, space folding allows for a whole range of physical effects, such as superlensing effect [51–56] and external cloaking in conjunction with anomalous resonances [46,49,57–60].

4. Conclusion

We have proposed to use stretched coordinates in order to design an elastic cloak bending the trajectory of in-plane coupled shear and pressure waves around an obstacle, concentrating them in its core, or focussing them. We investigated the transformed equations of motion for the Milton–Briane–Willis transformation gauge $\mathbf{u}'(r', \theta') = \mathbf{F}^{-t}\mathbf{u}(r, \theta)$ and the Brun–Guenneau–Movchan gauge $\mathbf{u}'(r', \theta') = \mathbf{u}(r, \theta)$ (see [41]). The former leads to Willis's equations with more extreme anisotropic parameters in the cloak than for the latter. However, the latter requires a transformed elasticity tensor without the minor symmetries, which is another hurdle for a metamaterial design.

We have studied various limiting cases for the value of a parameter in the considered radially symmetric linear geometric transforms. These transforms are applied to the design of neutral (invisibility) cloaks, elastic concentrators or cylindrical lenses.

We have numerically explored all the above for the gauge $\mathbf{u}'(r', \theta') = \mathbf{u}(r, \theta)$ leading to a non-fully symmetric transformed elasticity tensor, and have notably shown that a source located inside the anisotropic heterogeneous elastic coating seems to radiate from a shifted location, and can also lead to anamorphism.

We believe that our space folding based design of elastic cylindrical lenses can lead to an in-plane counterpart of the external cylindrical cloak for anti-plane shear waves introduced in [60] and applied periodically in [50].

We hope our results might open new vistas in cloaking devices for elastodynamic waves. Whereas their governing equations do not generally retain their form under geometric transforms, unlike for electromagnetic and acoustic waves, one can choose specific gauges that can make the transformed equations of motions easier to handle.

Declaration of competing interest

The authors declare that they have no known competing financial interests or personal relationships that could have appeared to influence the work reported in this paper.

Data availability

No data was used for the research described in the article.

Acknowledgments

M. Brun's work has been performed under the auspices of GNFM-INDAM.

References

[1] M. Farhat, S. Guenneau, S. Enoch, A.B. Movchan, Cloaking bending waves propagating in thin elastic plates, Phys. Rev. B 79 (3) (2009) 033102.
[2] M. Farhat, S. Guenneau, S. Enoch, Ultrabroadband elastic cloaking in thin plates, Phys. Rev. Lett. 103 (2) (2009) 024301.
[3] N. Stenger, M. Wilhelm, M. Wegener, Experiments on elastic cloaking in thin plates, Phys. Rev. Lett. 108 (1) (2012) 014301.
[4] D. Misseroni, D.J. Colquitt, A.B. Movchan, N.V. Movchan, I.S. Jones, Cymatics for the cloaking of flexural vibrations in a structured plate, Sci. Rep. 6 (1) (2016) 23929.
[5] D.J. Colquitt, M. Brun, M. Gei, A.B. Movchan, N.V. Movchan, I.S. Jones, Transformation elastodynamics and cloaking for flexural waves, J. Mech. Phys. Solids 72 (1) (2014) 131–143.
[6] L. Pomot, S. Bourgeois, C. Payan, M. Remillieux, S. Guenneau, On form invariance of the Kirchhoff–Love plate equation, 2019, arXiv preprint arXiv:1901.00067.
[7] M. Brun, D.J. Colquitt, I.S. Jones, A.B. Movchan, N.N. Movchan, Transformation cloaking and radial approximations for flexural waves in elastic plates, New J. Phys. 16 (2014) 093020.
[8] M. Morvaridi, M. Brun, Perfectly matched layers for flexural waves in Kirchhof–Love plates, Int. J. Solids Struct. 134 (2018) 293–303.
[9] A. Golgoon, A. Yavari, Transformation cloaking in elastic plates, J. Nonlinear Sci. 31 (17) (2021) 1–76.
[10] D. Schurig, J.B. Pendry, D.R. Smith, Calculation of material properties and ray tracing in transformation media, Opt. Express 14 (21) (2006) 9794–9804.
[11] U. Leonhardt, Optical conformal mapping, Science 312 (5781) (2006) 1777–1780.
[12] J.B. Pendry, D. Schurig, D.R. Smith, Controlling electromagnetic fields, Science 312 (5781) (2006) 1780–1782.
[13] A. Greenleaf, M. Lassas, G. Uhlmann, Anisotropic conductivities that cannot be detected by EIT, Physiol. Meas. 24 (2) (2003) 413.
[14] A. Greenleaf, Y. Kurylev, M. Lassas, G. Uhlmann, Electromagnetic wormholes and virtual magnetic monopoles from metamaterials, Phys. Rev. Lett. 99 (18) (2007) 183901.
[15] M. Kadic, G. Dupont, S. Enoch, S. Guenneau, Invisible waveguides on metal plates for plasmonic analogs of electromagnetic wormholes, Phys. Rev. A 90 (4) (2014) 043812.
[16] T.G. Philbin, C. Kuklewicz, S. Robertson, S. Hill, F. König, U. Leonhardt, Fiber-optical analog of the event horizon, Science 319 (5868) (2008) 1367–1370.
[17] S.W. Hawking, Black hole explosions? Nature 248 (5443) (1974) 30–31.
[18] J.B. Pendry, A.J. Holden, D.J. Robbins, W.J. Stewart, Magnetism from conductors and enhanced nonlinear phenomena, IEEE Trans. Microw. Theory Tech. 47 (11) (1999) 2075–2084.
[19] D. Schurig, J.J. Mock, B.J. Justice, S.A. Cummer, J.B. Pendry, A.F. Starr, D.R. Smith, Metamaterial electromagnetic cloak at microwave frequencies, Science 314 (5801) (2006) 977–980.
[20] S. Zhang, D.A. Genov, C. Sun, X. Zhang, Cloaking of matter waves, Phys. Rev. Lett. 100 (12) (2008) 123002.
[21] A. Greenleaf, Y. Kurylev, M. Lassas, G. Uhlmann, Approximate quantum cloaking and almost-trapped states, Phys. Rev. Lett. 101 (22) (2008) 220404.
[22] S.A. Cummer, D. Schurig, One path to acoustic cloaking, New J. Phys. 9 (3) (2007) 45.
[23] H. Chen, C.T. Chan, Acoustic cloaking in three dimensions using acoustic metamaterials, Appl. Phys. Lett. 91 (18) (2007) 183518.
[24] S.A. Cummer, B.-I. Popa, D. Schurig, D.R. Smith, J. Pendry, M. Rahm, A. Starr, Scattering theory derivation of a 3D acoustic cloaking shell, Phys. Rev. Lett. 100 (2) (2008) 024301.
[25] A.N. Norris, Acoustic cloaking theory, Proc. R. Soc. Lond. Ser. A Math. Phys. Eng. Sci. 464 (2097) (2008) 2411–2434.
[26] D. Torrent, J. Sánchez-Dehesa, Acoustic metamaterials for new two-dimensional sonic devices, New J. Phys. 9 (9) (2007) 323.
[27] M. Farhat, S. Guenneau, S. Enoch, A.B. Movchan, Cloaking bending waves propagating in thin elastic plates, Phys. Rev. B 79 (3) (2009) 033102.
[28] G.W. Milton, M. Briane, J.R. Willis, On cloaking for elasticity and physical equations with a transformation invariant form, New J. Phys. 8 (10) (2006) 248.
[29] D. Bigoni, S.K. Serkov, M. Valentini, A.B. Movchan, Asymptotic models of dilute composites with imperfectly bonded inclusions, Int. J. Solids Struct. 35 (24) (1998) 3239–3258.
[30] J.R. Willis, Variational principles for dynamic problems for inhomogeneous elastic media, Wave Motion 3 (1) (1981) 1–11.
[31] J.R. Willis, The nonlocal influence of density variations in a composite, Int. J. Solids Struct. 21 (7) (1985) 805–817.
[32] M. Brun, S. Guenneau, A.B. Movchan, Achieving control of in-plane elastic waves, Appl. Phys. Lett. 94 (6) (2009) 061903.
[33] H. Nassar, Y.Y. Chen, G.L. Huang, A degenerate polar lattice for cloaking in full two-dimensional elastodynamics and statics, Proc. R. Soc. Lond. Ser. A Math. Phys. Eng. Sci. 474 (2219) (2018) 20180523.
[34] M. Garau, M.J. Nieves, G. Carta, M. Brun, Transient response of a gyro-elastic structured medium: Unidirectional waveforms and cloaking, Int. J. Eng. Sci. 143 (2019) 115–141.
[35] Y. Achaoui, A. Diatta, M. Kadic, S. Guenneau, Cloaking in-plane elastic waves with Swiss rolls, Materials 13 (2) (2020) 449.
[36] A. Diatta, S. Guenneau, Controlling solid elastic waves with spherical cloaks, Appl. Phys. Lett. 105 (2) (2014) 021901.
[37] W.J. Parnell, Nonlinear pre-stress for cloaking from antiplane elastic waves, Proc. R. Soc. Lond. Ser. A Math. Phys. Eng. Sci. 468 (2138) (2012) 563–580.
[38] A.N. Norris, W.J. Parnell, Hyperelastic cloaking theory: Transformation elasticity with pre-stressed solids, Proc. R. Soc. Lond. Ser. A Math. Phys. Eng. Sci. 468 (2146) (2012) 2881–2903.
[39] W.J. Parnell, A.N. Norris, T. Shearer, Employing pre-stress to generate finite cloaks for antiplane elastic waves, Appl. Phys. Lett. 100 (17) (2012) 171907.
[40] M. Rahm, D. Schurig, D.A. Roberts, S.A. Cummer, D.R. Smith, J.B. Pendry, Design of electromagnetic cloaks and concentrators using form-invariant coordinate transformations of Maxwell's equations, Photon. Nanostruct.: Fundam. Appl. 6 (1) (2008) 87–95.
[41] A.N. Norris, A.L. Shuvalov, Elastic cloaking theory, Wave Motion 48 (6) (2011) 525–538.
[42] R.W. Ogden, Non-Linear Elastic Deformations, Courier Corporation, 1997.
[43] R.V. Kohn, H. Shen, M.S. Vogelius, M.I. Weinstein, Cloaking via change of variables in electric impedance tomography, Inverse Probl. 24 (1) (2008) 015016.
[44] D.J. Colquitt, I.S. Jones, N.V. Movchan, A.B. Movchan, M. Brun, R.C. McPhedran, Making waves round a structured cloak: Lattices, negative refraction and fringes, Proc. R. Soc. Lond. Ser. A Math. Phys. Eng. Sci. 469 (2157) (2013) 20130218.
[45] I.S. Jones, M. Brun, N.V. Movchan, A.B. Movchan, Singular perturbations and cloaking illusions for elastic waves in membranes and Kirchhoff plates, Int. J. Solids Struct. 69-70 (2015) 498–506.

[46] G.W. Milton, N.-A.P. Nicorovici, R.C. McPhedran, K. Cherednichenko, Z. Jacob, Solutions in folded geometries, and associated cloaking due to anomalous resonance, New J. Phys. 10 (11) (2008) 115021.
[47] Y. Zheng, X. Huang, Anisotropic Perfectly Matched Layers for Elastic Waves in Cartesian and Curvilinear Coordinates, Tech. Rep., Massachusetts Institute of Technology. Earth Resources Laboratory, 2002.
[48] F. Zolla, S. Guenneau, A. Nicolet, J.B. Pendry, Electromagnetic analysis of cylindrical invisibility cloaks and the mirage effect, Opt. Lett. 32 (9) (2007) 1069–1071.
[49] N.-A.P. Nicorovici, G.W. Milton, R.C. McPhedran, L.C. Botten, Quasistatic cloaking of two-dimensional polarizable discrete systems by anomalous resonance, Opt. Express 15 (10) (2007) 6314–6323.
[50] B. Meirbekova, M. Brun, Control of elastic shear waves by periodic geometric transformation: Cloaking, high reflectivity and anomalous resonances, J. Mech. Phys. Solids 137 (2020) 103816.
[51] N.A. Nicorovici, R.C. McPhedran, G.W. Milton, Optical and dielectric properties of partially resonant composites, Phys. Rev. B 49 (12) (1994) 8479.
[52] J.B. Pendry, Negative refraction makes a perfect lens, Phys. Rev. Lett. 85 (18) (2000) 3966.
[53] J.B. Pendry, S. Anantha Ramakrishna, Near-field lenses in two dimensions, J. Phys.: Condens. Matter 14 (36) (2002) 8463.
[54] J.B. Pendry, Perfect cylindrical lenses, Opt. Express 11 (7) (2003) 755–760.
[55] G.W. Milton, N.-A.P. Nicorovici, R.C. McPhedran, V.A. Podolskiy, A proof of superlensing in the quasistatic regime, and limitations of superlenses in this regime due to anomalous localized resonance, Proc. R. Soc. Lond. Ser. A Math. Phys. Eng. Sci. 461 (2064) (2005) 3999–4034.
[56] U. Leonhardt, T.G. Philbin, General relativity in electrical engineering, New J. Phys. 8 (10) (2006) 247.
[57] G.W. Milton, N.-A.P. Nicorovici, On the cloaking effects associated with anomalous localized resonance, Proc. R. Soc. Lond. Ser. A Math. Phys. Eng. Sci. 462 (2074) (2006) 3027–3059.
[58] G.W. Milton, J.R. Willis, On modifications of Newton's second law and linear continuum elastodynamics, Proc. R. Soc. Lond. Ser. A Math. Phys. Eng. Sci. 463 (2079) (2007) 855–880.
[59] O.P. Bruno, S. Lintner, Superlens-cloaking of small dielectric bodies in the quasistatic regime, J. Appl. Phys. 102 (12) (2007) 124502.
[60] S. Guenneau, B. Lombard, C. Bellis, Time-domain investigation of an external cloak for antiplane elastic waves, Appl. Phys. Lett. 118 (19) (2021) 191102.